Analysis of Local Microstructure and Hardness of 13mm gauge 2024-T351 AA Friction Stir Welds

D.P.P. Booth, M.J. Starink and I. Sinclair

Materials Research Group, School of Engineering Sciences, University of Southampton, Southampton, SO17 1BJ

ABSTRACT

The friction stir welding process has been used to join 13mm gauge 2024-T351 aluminium alloy plates together. A detailed microstructural study of the resulting weld was carried out using Differential Scanning Calorimetry (DSC), hardness testing, Scanning Electron Microscopy (SEM) and Electron Backscatter Diffraction (EBSD). DSC was used to explain the hardness results at a number of regions across the weld in terms of co-cluster dissolution and reformation and S phase formation, coarsening and dissolution. The "onion rings" structure found in the nugget weld was shown to be the result of a combination of the slight grain size variations and a change in nature and size of the particles present (i.e. intragranular versus intergranular). The variation in corrosion properties and hardness of the rings is discussed in terms of the local microstructure and quench sensitivities.

Keywords: friction stir weld, Al-Cu-Mg, co-clusters, precipitate, DSC, EBSD, hardness, fatigue

INTRODUCTION

The aerospace industry is showing significant interest in the use of advanced welding techniques in the fabrication of aerospace structures. One of the techniques that has shown promise is friction stir welding (FSW), a solid state process that has advantages over fusion welding in terms of reduced porosity, reduced residual stresses and less pre-weld preparation[1]. FSW is a solid-state joining technique in which a rotating tool is traversed along the weld path, plastically deforming (stirring) the surrounding material to form the weld and generating significant heat around the tool during the process[2]. During the FSW process, the rotating tool induces a complex plastic deformation in the surrounding material that varies as a function of the welding tool geometry. The maximum temperature achieved during the friction stir welding process is difficult to measure accurately, due to the high levels of deformation that occur in the weld region, but most researchers agree that the temperature reached is insufficient for global melting to occur, however several authors have suggested that incipient melting may occur[3,4]. The fine grain structure found in the centre of friction stir welds has often been ascribed to dynamic

recrystallisation[5], but detailed analysis using electron backscatter diffraction (EBSD) on a stop-action friction stir weld indicated that subdivision induced by deformation and dynamic recovery processes had occurred[6]. The grain refinement may be followed by some limited static grain growth[7]. However, questions concerning the microstructure development remain. Particularly, the origin of the so-called 'onion ring' structure developed in the weld nugget and the consequences of this banded structure for corrosion and fatigue properties continues to be researched[8,9]. Also a more quantitative interpretation of the local strength variations in relation to the microstructure development is being researched.

While a number of papers on the microstructure developed by the friction stir welding process have been published on a variety of aluminium alloys including heat treatable Al based alloys (e.g. AA6063[10], AA7075[11], AA209x[12] and AA2x24[13,14,15,16]) and non heat treatable alloys (e.g. AA5083[17]), these have tended to be on thinner gauges up to 7 mm, using single and double pass welds[18,19]. The current work has studied thicker 13 mm gauge 2024-T351 friction stir welds, using a combination of techniques including Differential Scanning Calorimetry (DSC), hardness testing, Scanning Electron Microscopy (SEM) and Electron Backscatter Diffraction (EBSD). Especially the application of DSC to systematically study the microstructure variations in thicker 2x24 friction stir welds is novel. The paper also contains some observations on the correlation between fatigue crack paths and local microstructure.

MATERIALS AND EXPERIMENTAL PROCEDURE

The current work is based on a full penetration weld in 13mm gauge 2024-T351 plate welded parallel to the longitudinal direction of the plate by Airbus UK, weld tool design and welding conditions are proprietary. The weld was left to naturally age for several months.

Samples for optical microscopy were prepared using standard silicon carbide grinding up to 4000 grit, followed by mechanical polishing with 1μm diamond paste using Struers Red lubricant, and 0.02μm OPS solution (alumina suspension). Samples for Electron Backscattered Diffraction (EBSD) were first mechanically polished to 0.02μm OPS as describe above, and subsequently electropolished by immersion in a 10% nitric acid in methanol solution cooled to -30°C; polishing was carried out at 30V for between 3 and 5 seconds.

An Olympus BH-2 microscope was used for the optical microscopy. SEM was conducted on a Jeol 6500 FEG-SEM. The EBSD orientation maps were obtained using the commercial HKL Channel 5 system, with an accelerating voltage of 20keV, specimen tilt of 60°, working distance of 30mm and an increment distance of 0.5μm between points.

Microhardness was obtained with a load set to 1kg and dwell time of 15s. All testing was carried out on a surface polished to 0.02μm OPS finish.

Differential Scanning Calorimetry (DSC) was performed on a Perkin Elmer Pyris 1 heat compensation DSC on 3-4 mm diameter specimens. The DSC specimens were obtained from 2 and 10mm below the crown (top) surface at a range of locations across the weld. The reference sample was an empty pure aluminium sample pan, tests were carried out using a nitrogen gas flow and heating rate of 10°C/min. Baseline correction procedures are outlined in[20], all presented DSC curves reflect the heat flow due to reactions. Due to the strong differences in the DSC curves from the different samples, slight inaccuracies in baseline determination in the order of ±5 10^{-3} W/g may remain.

The fatigue test specimens were all cut transverse to the welding direction. The crown surface of all specimens was skimmed by 2 mm to remove any weld features: this was carried out using a standard milling machine taking very small amounts of material off in each pass to minimise any residual stress that may be introduced by the deformation associated with machining. The length of the specimens was 300 mm, this enabled the entire weld affected region to be tested. Specimens were tested with a range of widths, from 25 to 50mm. All tests were carried out in four point bend at 10Hz with a centre roller spacing of 90mm, with the outside rollers another 40mm beyond that.

RESULTS

Macrostructure

The overall weld structure is illustrated by the optical micrograph montage of a cross section normal to the weld in Fig. 1 and a magnified section of one half of the weld in Fig. 2. The following features are observed:

- a well defined central nugget exhibiting a distinct annular banded (or 'onion ring') region
- flow of the parent grain structure in and around the weld nugget
- a 'flow arm' region between the nugget and the surface on which welding was carried out penetrating to a depth of ~5mm below the weld crown; this is deeper as a proportion of the overall thickness than seen in most of the thinner welds found in the literature[21].
- the thermo-mechanically affected zones (TMAZ) are observed over the entire width of the weld region, and, in particular, for the retreating side of the weld in Fig. 2 (i.e. the side of the weld where the direction of probe rotation and the work piece traverse direction are opposite).
- a small region of grain flow upwards into the weld toe, extending some 1 – 2mm into the main body of the plate.

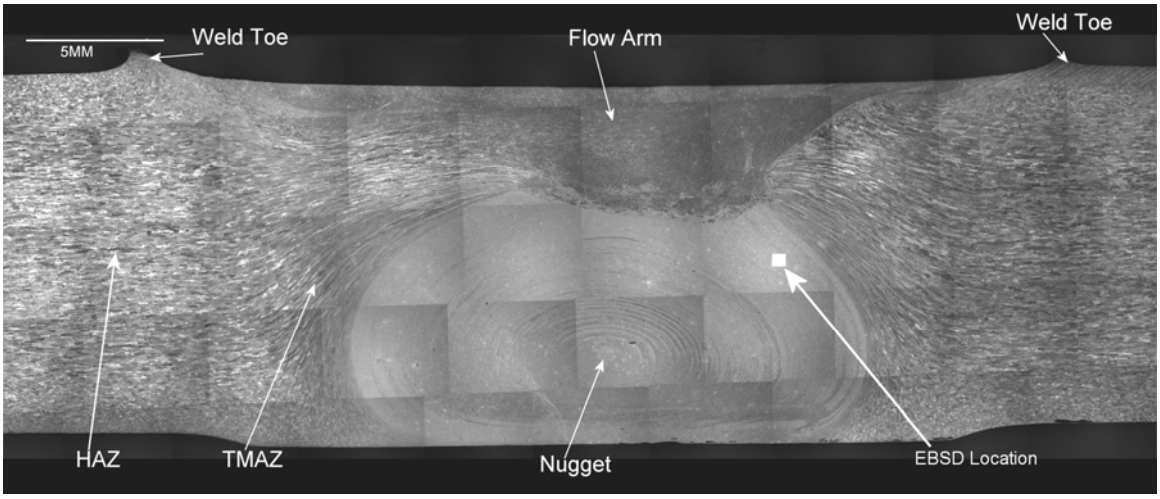

Fig. 1 Optical macrograph of friction stir welded 13mm gauge 2024-T351 plate (etched and viewed in crossed polarisers).

The line traces shown in Fig. 3 correspond to individual hardness profiles through the weld nugget (near its centre) and through the flow arm (approx. 2mm below the plate crown surface). Linear regression analysis indicates that the hardness decreases slightly from about 100mm to about 60 to 70 mm from the weld centre line. In approaching the weld line further, both traces exhibit a rise in hardness from the parent plate hardness level to a peak hardness at about 45mm from the weld centre line. This is followed by a gradual decline in hardness to a minimum at about 15mm either side of the weld line. There is then a steep rise in hardness to a central plateau of intermediate hardness. The hardness trace through the weld nugget in Fig. 3 shows a small but distinct dip in the central plateau region. Further mapping of hardness confirmed that the slight peak in hardness at the outer edge of the heat affected zones (HAZ) is indeed consistent through the whole plate thickness[22].

The apparent edge of the flow arm region in the hardness does not occur at the apparent interface in the grain structure; rather it is extended out into the TMAZ. This is highlighted in Fig. 2 showing a local region in the transition zone from the HAZ, to the TMAZ, to the flow arm. The hardness indents that may be seen in the micrograph show that the minimum in hardness occurs in the HAZ (below the weld toe) where the parent grain structure has essentially been retained (a mild grain rotation has occurred). The figure shows that whilst hardness levels rise sharply further into the weld, there is little or no variation in hardness as the trace passes the interface in grain structure between the deformed grains of the TMAZ and the very fine structure of the flow arm.

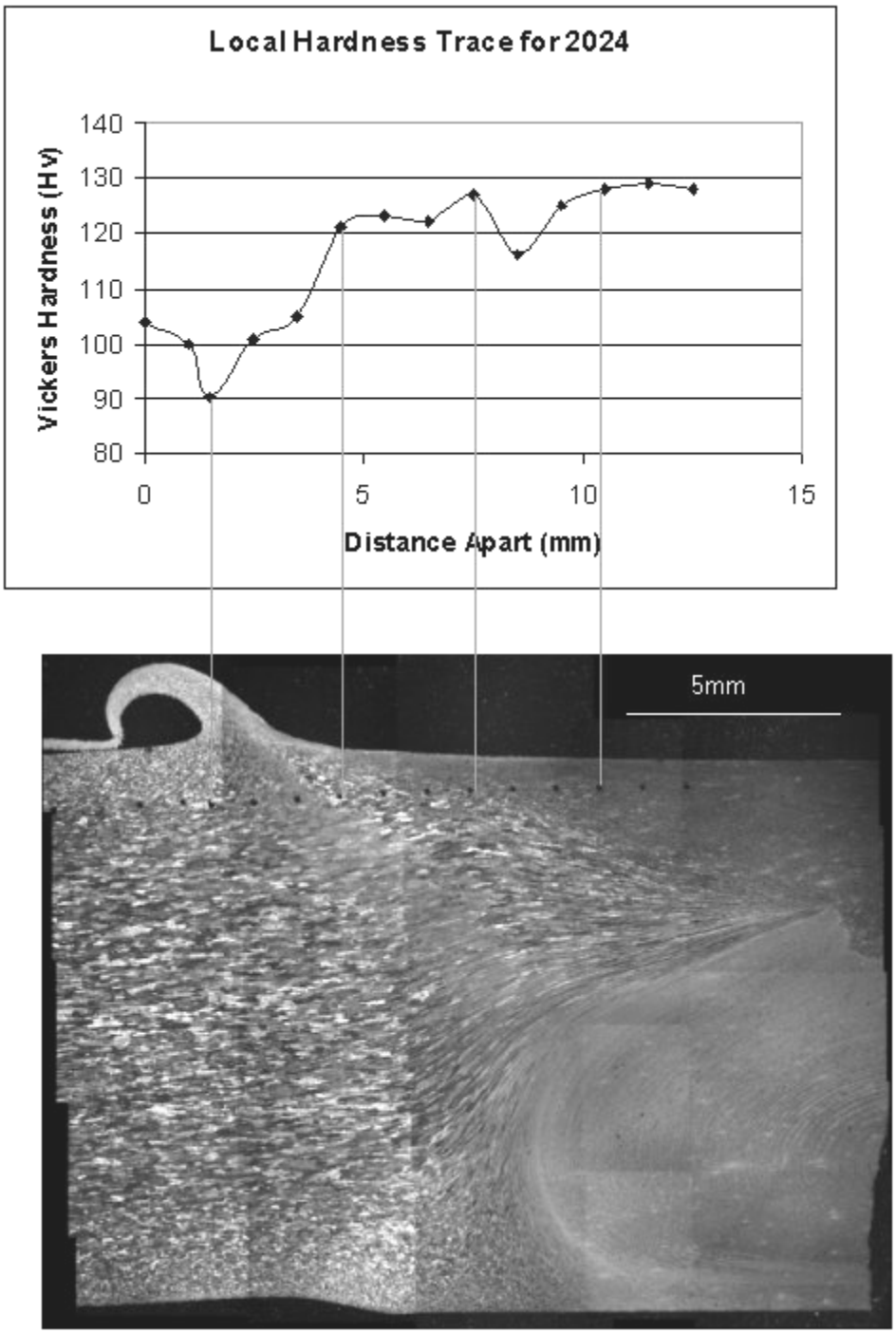

Fig. 2 Local micro-hardness variations in relation to the weld flow arm grain structure.

Hardness Characteristics

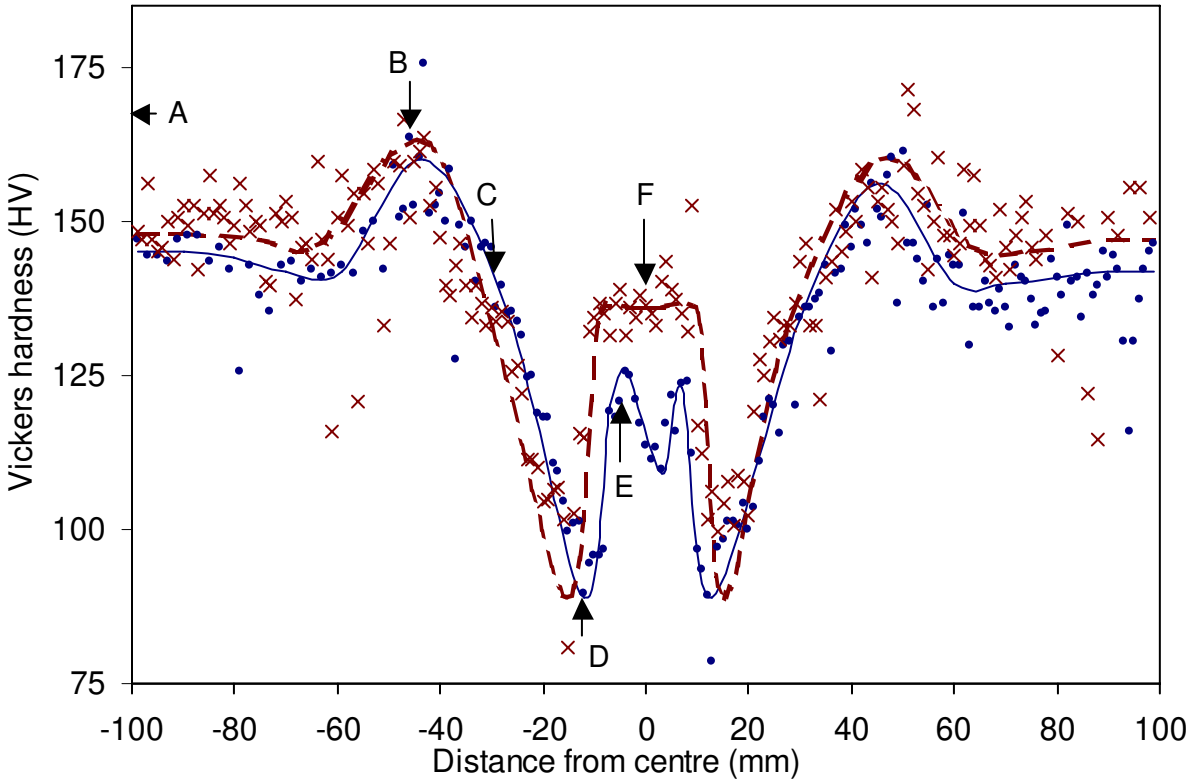

Fig. 3 Characteristic hardness traces for 2024 friction stir welds taken from 4mm below the crown surface (●) and 11mm (×) below the crown surface. Locations of the DSC samples are indicated (A-F).

Differential Scanning Calorimetry

Differential Scanning Calorimetry (DSC) was carried out on samples taken from various locations on two lines normal to the welds, one through the flow arm and one through the weld nugget. The location (marked A to F) of each of the DSC specimens is shown on the hardness traces in Fig. 3. Fig. 4 shows the DSC curves for all of the specimens. Looking at the parent plate trace (A) the general trend of the important features can be ascertained. There is little heat flux to approximately 150°C, where there is an endothermic effect that is consistent with dissolution of Cu-Mg co-clusters[23,24,25,26,27*], this is followed by an exothermic peak at about 250°C which may be attributed to the formation of S phase[25,28]. There is a long endothermic region above ~300°C corresponding to dissolution of previous phases. There are a number of

[*] Some researchers prefer the term Guinier-Preston-Bagaryatsky (GPB) zones.

sharp endothermic peaks consistent with the onset of incipient melting between 500°C and 515°C [29,30,31].

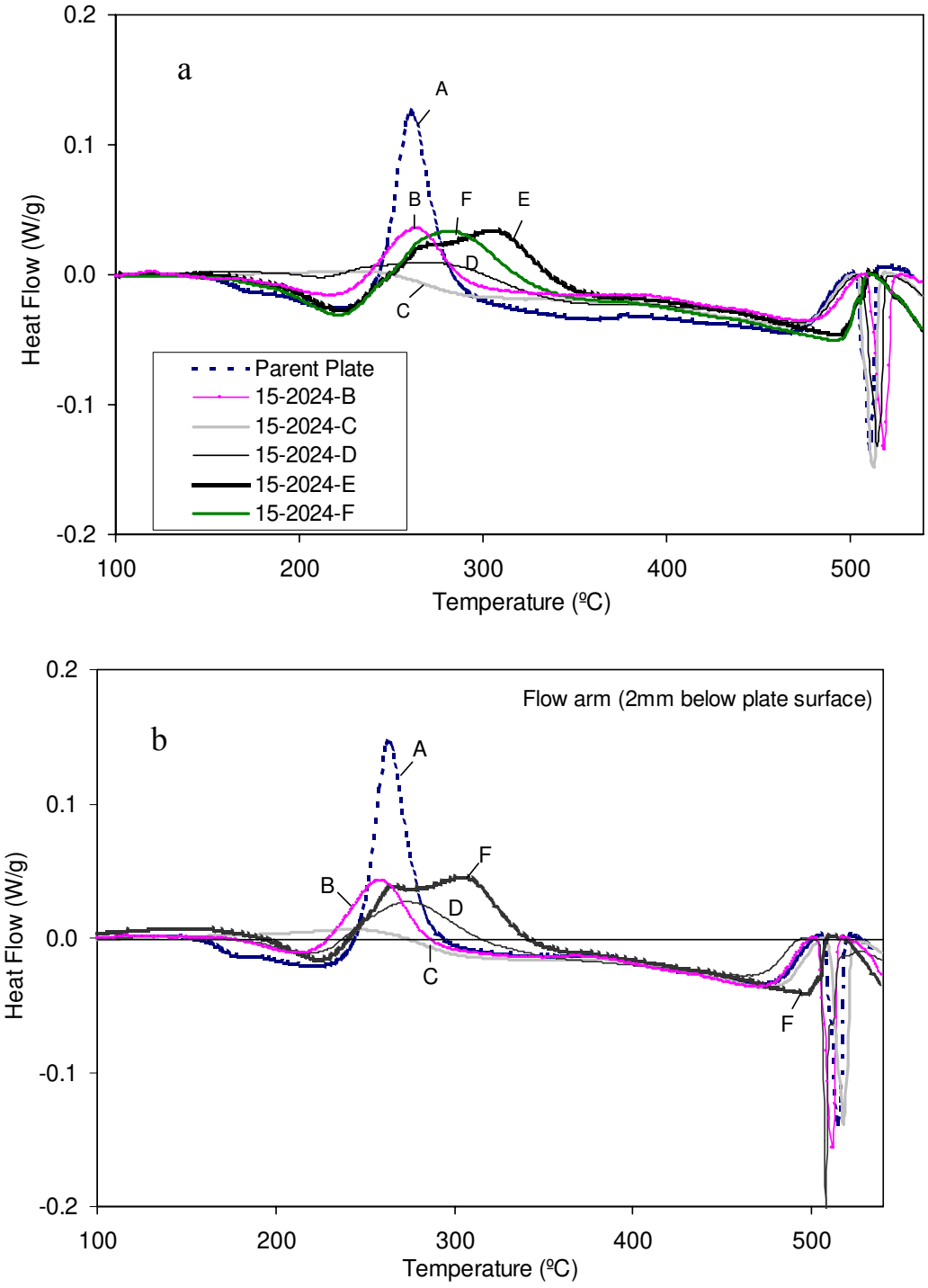

Fig. 4 DSC curves of samples extracted from a line through a) the centre of the weld nugget, and b) the flow arm. A=parent plate, B=maximum hardness, C=approximate middle of hardness drop, D=hardness minimum, E=local hardness maximum at edge of weld nugget and F=weld centre.

Looking at the low temperature reactions for the other locations across the weld, starting with trace B (which corresponds to the HAZ peak in hardness), a significant amount of S phase appears to have been precipitated before the run (with a corresponding drop in zone content), accounting for the increase in hardness via a degree of artificial ageing. Trace C (located on the decrease in hardness) shows very little co-cluster dissolution and practically all of the available S phase appears to have been precipitated. At the hardness minimum (D) there is evidence of some co-cluster formation, suggesting a degree of resolutionising and reageing. In the weld centre (F) there is a significant increase in the co-cluster dissolution peak, (c.f. location D). It is also interesting to note a distinct split in the intermediate temperature exothermic effect (250-350°C). Whilst the origins of this effect has not been explicitly checked in this work, recent reports by Lefebvre *et al*[32] and Wang *et al*[33] suggest the possible formation of Ω (Al_2Cu) phase under slow cooling conditions in 2024 welds and bulk material. Thus further formation of Ω (Al_2Cu) phase could contribute to the apparent additional reaction in the present slow cooled weld region. Alternatively, the occurrence of S phase in two orientation relationship variants (which have been evidenced by TEM[34,35]) may influence the appearance of the double exothermic effect.

For locations (B) and (C) the high temperature incipient melting effects are essentially the same as the parent plate trace (A), with a dissolution reaction continuing up to about 498°C, and the onset of incipient melting occurring at 504°C. This incipient melting reaction is typically due to relatively coarse intermetallic phases[20], and the lack of change indicates that outside of the flow arm these particles are not affected by the weld processing. DSC data obtained from point (D) shows a significant change in the incipient melting effect, with the onset increasing to about 510°C and a secondary effect appearing with peak at about 518°C. The DSC data obtained from point (E) (centre line of flow arm) is very different from all other curves, with the endothermic dissolution effect continuing until about 508°C and no evidence of incipient melting up to 540°C. A gradual onset of melting of the Al rich matrix from about 530°C appears to occur for all samples, but due to potential inaccuracies of the baseline this can't be confirmed from the present data.

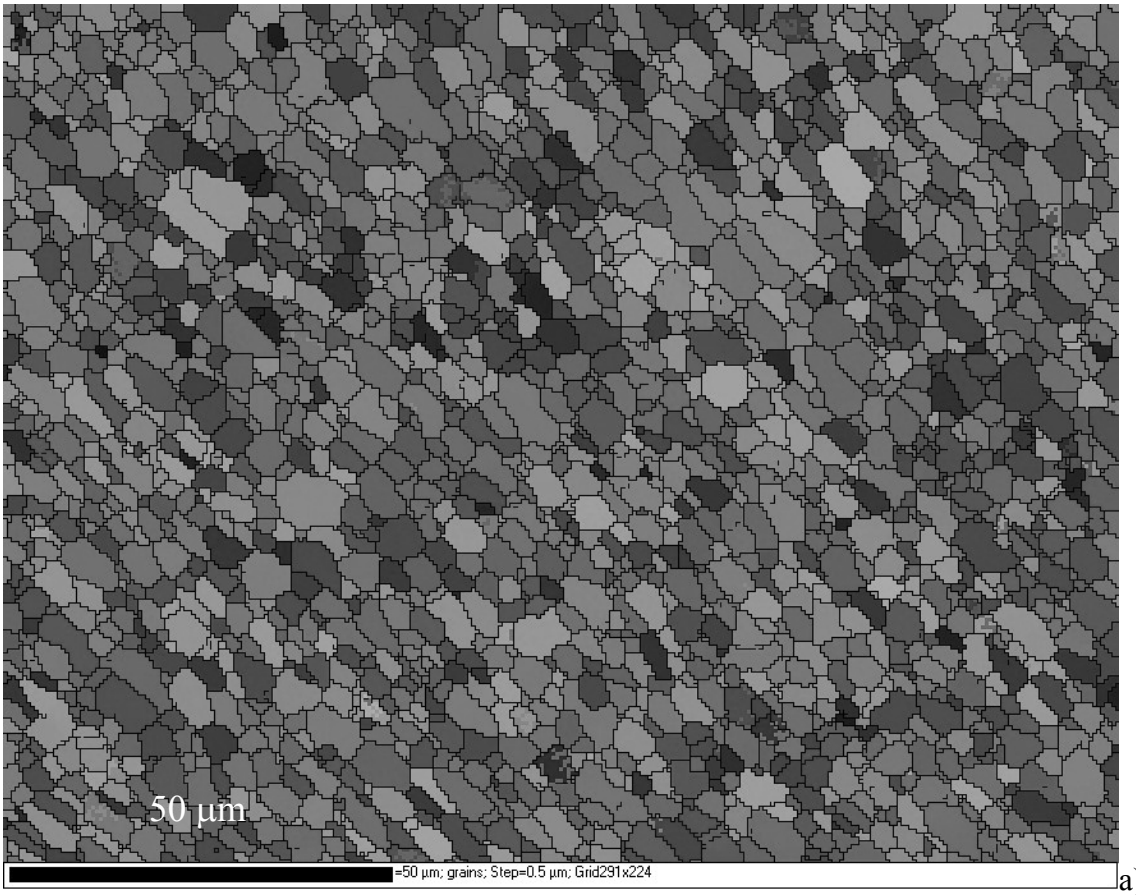

a)

b)

Fig. 5 Maps of nugget region indicated in Fig. 1: a) EBSD orientation map and b) contour map of maximum grain feret dimensions.

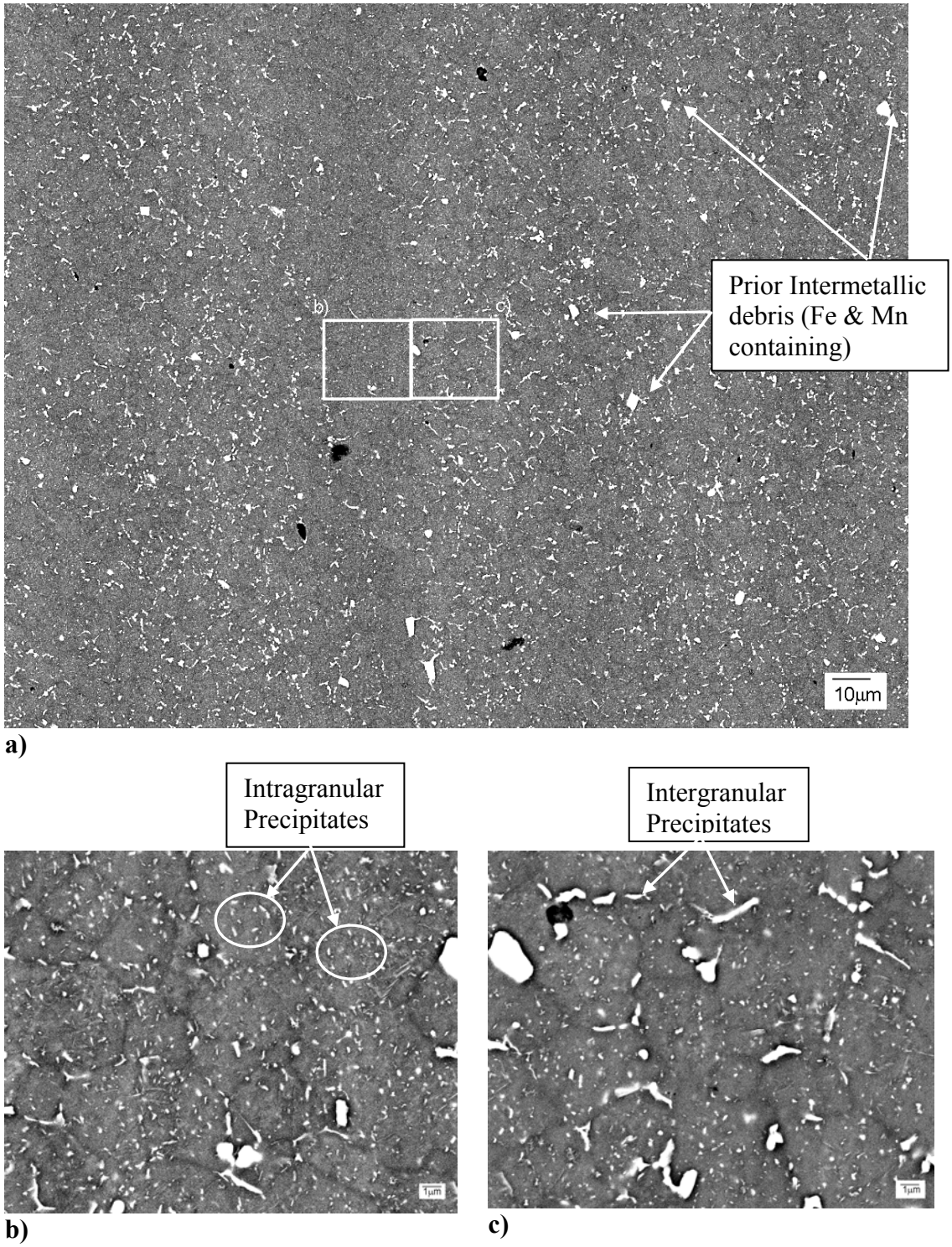

Fig. 6 FEG-SEM BEI images across an apparent band in intermetallic density within the weld nugget; a) low magnification image showing location of images b) and c).

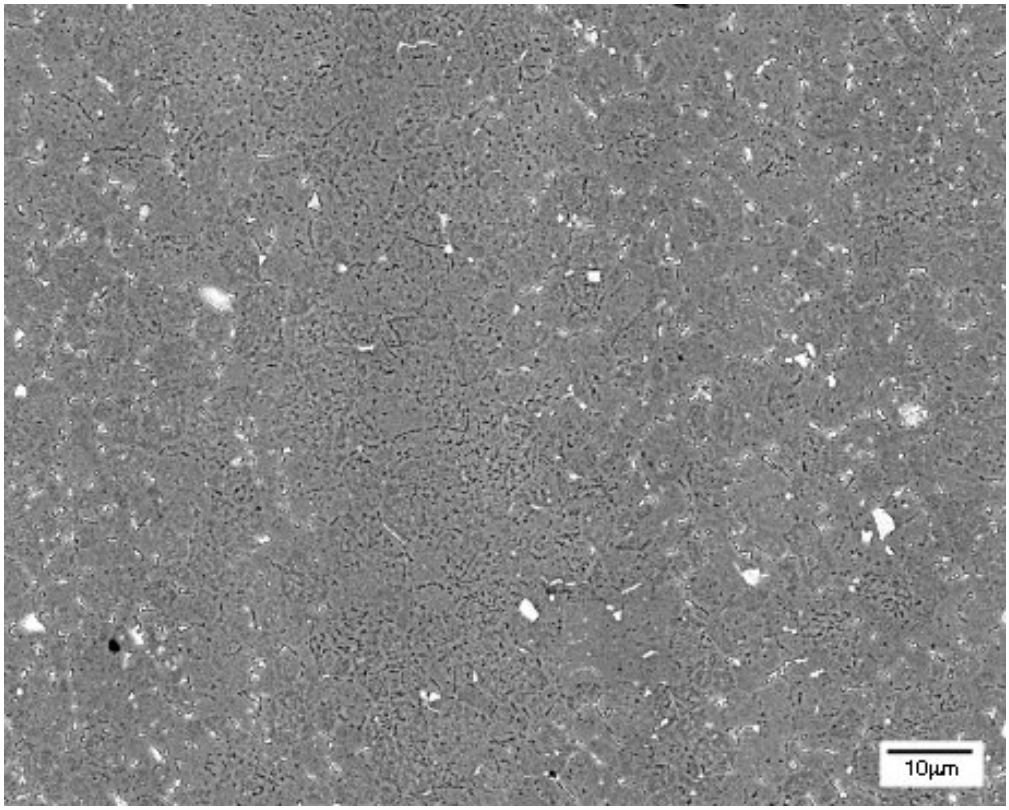

Fig. 7 SEM BEI image of the etched weld nugget region, covering a similar area to that shown in Fig. 6.

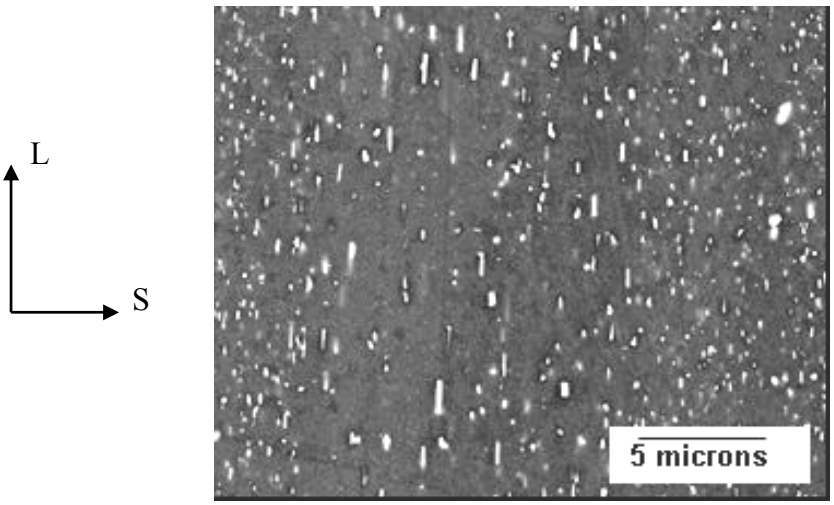

Fig. 8 SEM BEI image showing the heterogeneity of dispersoid particle distribution in parent plate 2024-T351[36]

The characteristically fine grain structures of the flow arm and weld nugget regions were studied using optical microscopy. The average grain size of both flow arm and nugget regions was estimated (using an average of the horizontal and vertical linear intercepts) to be of the order of 3-4 μm, with the nugget typically showing a slightly finer structure (i.e.~3 μm). In terms of the onion ring structure that was evident macroscopically in the weld nugget (i.e. as in Fig. 1), optical microscopy did not reveal any distinct changes in grain dimensions between the bands. Further analysis of the grain size in the nugget region was performed at the location indicated in Fig. 1 using EBSD mapping carried out in the FEG-SEM. The resulting map (Fig 5a) revealed no systematic grain size variation that correlated with the bands seen in Fig. 1. (It may be noted that ~85% of boundaries were noted to be high angle (>12°), in keeping with the results reported by Hassan *et al*[37]). Fig. 5a shows that grains are generally elongated in a direction about 45° to the horizontal axis, and this is further confirmed by determination of grain size with the linear intercept method applied parallel, perpendicular and ±45° to the horizontal axis (i.e. the transverse direction to the weld line) (Table 1). Variations in structure are further highlighted in the plot of maximum feret directions in Fig. 5b; light regions correspond to a larger grain size than the darker regions. This variation appears to show some evidence of patches of varying grain size, however, the scale and consistency of the bands was not obviously connected with the macroscopic onion ring bands seen in Fig. 1. The EBSD results reported in Table 1 for the grain sizes taken from Fig. 5a and equivalent EBSD maps of the flow arm support the average grain size measurements reported from the optical observations, with the flow arm having a coarser grain structure than the nugget (average grain sizes via EBSD of 5.1 μm and 3.1 μm in the flow arm and nugget respectively).

A detailed study of un-etched and etched specimens was carried out in the FEG-SEM. The location of Fig. 6a was close to the advancing edge of the weld nugget, approximately level with the nugget centre, with the location of the subsequent images in Fig. 6 being marked in Fig. 6a. Coarser intermetallic particles are marked in Fig. 6a: these are commonly seen to be Fe and Mn containing, presumably remaining from the parent intermetallic population. A band in the particle distribution is clearly evident in Fig. 6a; in particular, a band of reduced intermetallic content is seen to run vertically, slightly to the left of centre in the image. At higher magnification (Fig. 6b and c) the presence of fine (≤0.5μm) evenly dispersed intragranular particles is noted in Fig. 6b, whilst in Fig. 6c more coarse (~1-2μm) intergranular particles are evident given the scale and morphology of these particles, and their apparent composition (EDX indicates the intergranular particles are Cu and Mg rich) these particles are presumed to be precipitates from the weld thermal cycle (probably S, with the present DSC results and the results of Lefebvre *et al*[25] suggesting the possible presence of θ`/Ω phase). Fig. 7 shows a similar region as that shown in Fig. 6a), etched with Keller's reagent. Distinct intragranular attack takes place in the central region/band, consistent with preferential etching of the fine particles. Overall it was noted that the macroscopic onion ring structure of the nugget region was closely associated with these local variations in intergranular and intragranular particle content, with those regions that

appear dark in macroscopic images (such as Fig. 1) being associated with an increased incidence of the intragranular particle bands and their associated intragranular etching when treated with Keller's reagent.

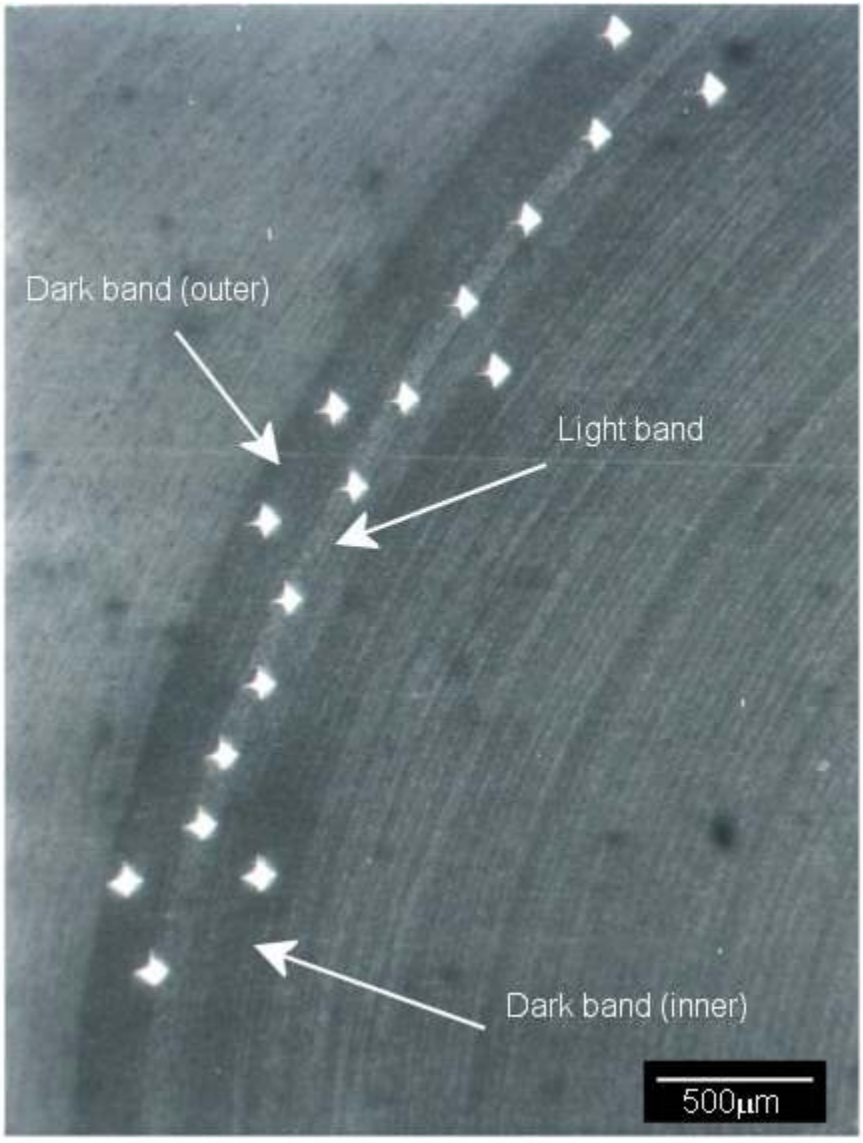

Fig. 9 Hardness variation between bands in the weld nugget region. The light band is consistently harder than the surrounding dark bands by ~7HV

Fig. 10 Macrograph showing the fatigue crack path down through the weld region.

Grain Structure of the Weld Region

Noting the differences between the bands reported above, it is of course interesting to consider the potential strength differences that might arise locally. Hardness indentations made in the light band and the dark bands of the weld nugget region (Fig. 9) revealed that the light band is consistently harder than the surrounding dark bands by ~7HV (which corresponds to a proof strength variation of ~20MPa). (It should be noted that this is expected to be a lower bound given the comparative size of the hardness indents to the bands present, therefore some material outside the bands is also likely to be sampled.) The light bands shown here by optical microscopy have a higher incidence of coarse intergranular precipitates while the dark bands contain more of the fine intragranular precipitates. Sutton *et al*[8] also noted a variation in hardness between the onion ring bands by values of the order of ~6HK (Knoop hardness).

Location	Angle to x-axis in Fig. 5	Axis 1 grain dimension (μm)	Axis 2 grain dimension (μm)	Average grain size (μm)	Aspect Ratio
Nugget (	0°	2.5	2.7	2.6	0.9
Fig. 5a)	45°	3.9	2.3	3.1	0.6
Flow arm	-	3.5	6.7	5.1	0.5

Table 1 Grain size taken from EBSD map at 0° and 45° to the horizontal axis in Fig. 5a) for nugget and for the flow arm.

Fatigue crack growth paths

Five failed fatigue test samples of the weld were analysed for evidence of the banded microstructure on crack paths. For the five specimens tested, two forms of failure were identified: (i) tests where failure occurred outside of the flow arm/nugget region, and (ii) tests where failure occurred from within the actual weld material (identified here as 'over' the nugget region). In this work we will consider only the two failures that occurred over the weld nugget region. (Further results, with comparison of the different failure modes and fatigue lives, will be presented elsewhere.) Fig. 10 shows a general view of the fracture surface of the region close to the initiation point for one of the failures over the nugget region; the crack growth through the weld flow arm (top ~2 mm) showed some minor deflections from a nominal mode I path. The curved nature of the crack growth around the nugget region can clearly be seen in the lower parts of Fig. 10. The deflection of the crack path forms a curve that closely follows the macroscopic onion ring structure of the nugget region. Sections from both halves of the failed sample showed that crack growth had occurred just within the nugget, rather than at the nugget/TMAZ interface. Fig. 11 shows a local step in the crack path (i.e. a region running perpendicular to the overall banding structure of the nugget). There is evidence this step has occurred across a region of lower intermetallic content, with the dominant growth direction (i.e. following the onion-ring structure) being resumed in a region of higher intermetallic content.

DISCUSSION

Recently we published detailed work on predictive modelling of microstructure development and strength of Al-Cu-Mg FSW and fusion welds[26,38, 39,]. This work showed that local strength is dominated by the Cu-Mg clusters and the S phase. Changes in strength and hardness of friction stir welds strength are due predominantly to primary precipitation, coarsening, resolution and re-precipitation, with some changes due to localised incipient melting and re-solidification. In the following discussion of the present findings we will make use of these modelling results.

In terms of local matrix precipitation effects, the local hardness in welds in a heat treatable alloy is clearly dependent on the thermal cycles caused by the welding process. The predominant drop in hardness from the parent plate into the HAZ/TMAZ is due to the coarsening of strengthening precipitates (i.e. overaging) during the heat cycle[25,38]. This is supported by the DSC results shown in trace C, in Fig. 4, from samples taken at the initial drop in hardness moving from the parent plate towards the weld line. These curves show very little co-cluster dissolution and no higher temperature precipitation, indicative of a fully aged structure. DSC results shown in trace C, in Fig. 4, which is close to the minimum in hardness, shows an increased amount of co-cluster dissolution and small, broad precipitation effect at around 250-300°C, indicating that some solute was available for precipitation after the weld pass. The low strength at this point must then be attributed to heavy coarsening of S phase and/or heterogeneous precipitation during the welding heat cycle[25,26,38], with the subsequent co-cluster precipitation providing only a limited contribution to strength. At positions E and F, the substantial co-cluster dissolution and S phase formation effect that is substantially enhanced with comparison to position D indicate increasingly effective resolutionising and subsequent natural ageing of the material.

The high temperature portions of the DSC curves revealed that in the TMAZ close to the flow arm, the incipient melting temperature of the welded material had increased, whilst for the weld centre specimens (E and F) the incipient melting in the range up to 530°C is entirely eliminated (Fig. 4). It is thought that this is due to break up of particles and mechanical and thermal homogenisation resulting from the action of the weld tool. To elucidate this, we should first note that incipient melting occurs when on increasing the temperature the local phases present and their compositions reach a eutectic composition. These local phases present and their compositions are usually related to remnants of the solidification structure that have not been fully homogenised during subsequent treatment or to grain boundary precipitates. In as-cast alloys, incipient melting during heating will occur first at the temperature of the final eutectic solidification reaction ($T_{eut,f}$). An homogenising heat treatment (performed just below $T_{eut,f}$) can redistribute the alloying atoms in such a way that melting will not occur at $T_{eut,f}$, but melting at a higher temperature can then be possible. The extension of the dissolution effect until about 508°C for DSC experiments on samples taken from point E is thought to result from coarser intermetallic particles (esp. S phase) being broken into smaller fragments due to the mechanical action of the FSW tool. Whilst the original, coarse particles will dissolve very slowly, given very small, possibly undetectable heat effects, these smaller fragments will be able to dissolve relatively fast during the DSC run. This mechanism explains the appearance of the extended dissolution effect, and can also explain the absence of an incipient melting effect, as the enhanced dissolution of any phases that cause the incipient melting in DSC samples from other locations, will reduce or eliminate incipient melting.

The microstructure of the bands in the nugget region has been studied by a number of workers and the following features related to the onion ring features have generally been identified:

1. Variation in intermetallic particle density between the bands,
2. Variation in grain size/shape.

For the present 13 mm welds, it is clear that grain size variation within the weld nugget was quite limited, corresponding to no more than 1-2μm. Whilst not all authors have reported such variations, these results are consistent with work by Mahoney *et al.* [11] on FSW 7075. It may also be noted that the grain structure of the present welds was aligned to some extent with the banding of the weld. The alignment is however relatively mild, with grain aspect ratios of the order of ~0.6, i.e. very much less than those found in common wrought Al alloy products. It should also be noted that the local variations in the grain structure identified in the present welds are not "continuous" features, but are quite patchy compared to the extended nature of the onion rings seen in Fig. 1.

The understanding of formation of onion rings is far from complete, and various possible mechanisms have been proposed[2]. The present FEG-SEM observations revealed variations in particle size and distribution across the weld nugget region that are associated with the onion ring features. In particular, 3 populations of particle were identified; i) larger intermetallic debris from the parent material, up to ~3-4μm in diameter, ii) intergranular precipitates of the order of 1-2μm, and iii) intragranular precipitates up to ~0.5μm. Both in this work and previous work[40] a difference in the intermetallic distribution between the bands in the nugget region was identified. The intragranular particle observations and differential etching effects noted in Fig. 7 suggest a local variation in matrix precipitate condition between the bands. In considering the probable cause of the local differences in hardness and etching effects between the bands we take into account that in the parent plate the distribution of dispersoid particles and coarser intermetallic particles which are remnants of the final stages of solidification are distributed inhomogeneously (see Fig. 8 [36]). It is thought that the breaking up of these course particles and particle clusters by the fast rotating welding tool results in the heterogeneous banded distribution of finer particles[8,41,45]. This is due to material being effectively picked up and deposited in layers that are mechanically coupled to the tool rotation during each cycle [2,42]. The cooling rates achieved in the TMAZ at about 350 to 400°C (the temperature range where precipitation on cooling would occur) are typically in the order of 10°C/s, which is higher than the rate (~1°C/s) at which a 2024 alloys starts to show some quench sensitivity but well within the range of cooling rates at which a 2124MMC, which will contain many particles and particle debris, shows substantial quench sensitivity[43,44]. Thus locations where fine fragments of intermetallic particles are present can show substantial quench sensitivity and intragranular precipitation (especially of S-phase) can be expected. Such precipitation would be expected to interact with etching in Keller's reagent, i.e. the more heavily etched bands would be consistent with greater intragranular precipitation. This mechanism is also consistent with the observed differences in hardness between the bands, as precipitation during cooling will cause reduced formation of co-clusters, which are the main hardening mechanism. The measured hardness differences between the bands of 7HV

correspond to a proof strength difference of about 20 MPa. Using the model for strengthening of Starink and co-workers[23,24,26] this strength differential would correspond to about 14% of the Cu and Mg present in the alloy being incorporated in the precipitates formed during cooling. Whilst the above interpretation is generally consistent with results and is reasonable in qualitative terms, it should be noted that the link between intermetallic particles and quench sensitivity is a complex one, in which apart from precipitation during cooling, also vacancy loss during cooling and subsequent alteration of low temperature precipitation can play a role. It is also noted that the onion ring bands disappear when the rotational speed of the tool is increased[45], consistent with more effective mixing and homogenisation of the weld material.

It is also noted that the precipitation peaks in the DSC curves for the samples obtained in and near the flow arm (Fig. 4) and the weld nugget (presented elsewhere [22]) are broader than those observed in samples from fusion welds. This is likely to be caused by the onion ring features which cause local variations in precipitation kinetics between the bands.

In addition to the above mechanism, the incidence of adiabatic shear bands (ASBs) may be anticipated in high strength aluminium alloys[46] under conditions of severe temperature and strain rate (of the order 500°C and 10 /s respectively), with clear implications for homogeneity of temperature and deformation process. Such temperature and strain conditions have indeed been reported within the literature in relation to friction stir weld processing, but have not as yet been explicitly linked (to the best knowledge of the authors) to the presence or absence of ASBs in friction stir welds. Notwithstanding the origins of deformation banding within the nugget, the fact that grain size variations may be limited (as seen here) is consistent with the assertion of Hassan *et al*[37] and Frigaard *et al*[47] that the final nugget grain dimensions must be controlled by growth rather than strain/strain rate, although further assessment and quantification of weld process conditions is clearly required to verify the presence of such complex mechanical and microstructural interactions.

A distinctive feature of crack propagation was the macroscopic crack deflection closely following the onion ring pattern of the nugget region. As such, it is evident that such flow features of the weld represent intrinsic weakness within the welds. Given the current evidence, the deflected nature of crack growth in the weld nugget region may be identified as a consequence of propagation being channelled by variations in matrix microstructure and/or the mechanical influence of crack propagation between regions of high and low yield stress (cracks tending to deflect back into a soft material on approaching a hard material interface, as the crack tip plastic zone is constrained on entering the harder material). The most prominent, direct microstructural effect would appear to be the presence of intermediate sized intermetallic particles (up to 2μm). Whilst extensive fractographic examination did not reveal significant void growth from these particles, it may be presumed that they still provided some favourable path for crack growth to

occur. The fact that such particles were often intergranular in character does not appear to have been critical however, as much of the deflected crack growth was seen to be transgranular.

Monotonic crack propagation along onion ring bands in the weld centre has been reported by Sutton et al[8] for 2024-T351 friction stir welds in 6.25mm gauge specimens, under mixed-mode I/II loading with a through thickness pre-crack in the weld centre parallel with the welding direction. Sutton et al[8] attribute the deflected crack growth along the bands to larger particle (~5μm+) density differences. They suggest that growth is along coarse particle rich bands consistent with the monotonic load condition as opposed to the cyclic failure of the present work.

Overall it may be identified from the present results that preferential failure/crack deflection at the nugget `onion ring` features may be linked to a combination of failure via the intermediate intermetallic particle distribution formed by heterogeneous precipitation during the weld cycle, and mechanical contributions of strength differentials between the onion ring bands. It may be noted however that these factors are intimately linked, as heterogeneous precipitation process may largely determine local flow strength, with the two factors therefore being difficult to strictly separate.

SUMMARY

The 13 mm gauge 2024-T351 friction stir weld macrostructure is comparable to friction stir welds reported in the literature for thinner gauge heat treatable aluminium alloys in that a banded weld nugget is evident, along with the presence of flow arm and TMAZ regions. The grain structure in the weld nugget is reasonably fine, with a grain size of ~3 μm, with limited grain elongation parallel to the onion ring bands. No significant change in grain size was associated with the onion ring banding. The intermetallic particles within the nugget (and flow arm) were much reduced in size and redistributed compared to those of the parent plate, and there is evidence of systematic variation in both size and nature (intergranular versus intragranular location) of the fine intermetallic particles that are associated with the onion rings of the weld nugget.

The hardness traces show a central plateau and a minimum on either side. The hardness variation between the bands of the nugget region appears to be related to differences in intermetallic distributions and is likely to be caused by enhanced quench sensitivity due to the presence of particles in bands that were fragmented by the action of the fast rotating tool.

ACKNOWLEDGEMENTS

The authors would like to thank EPSRC for their financial support and Airbus UK for financial support and the material.

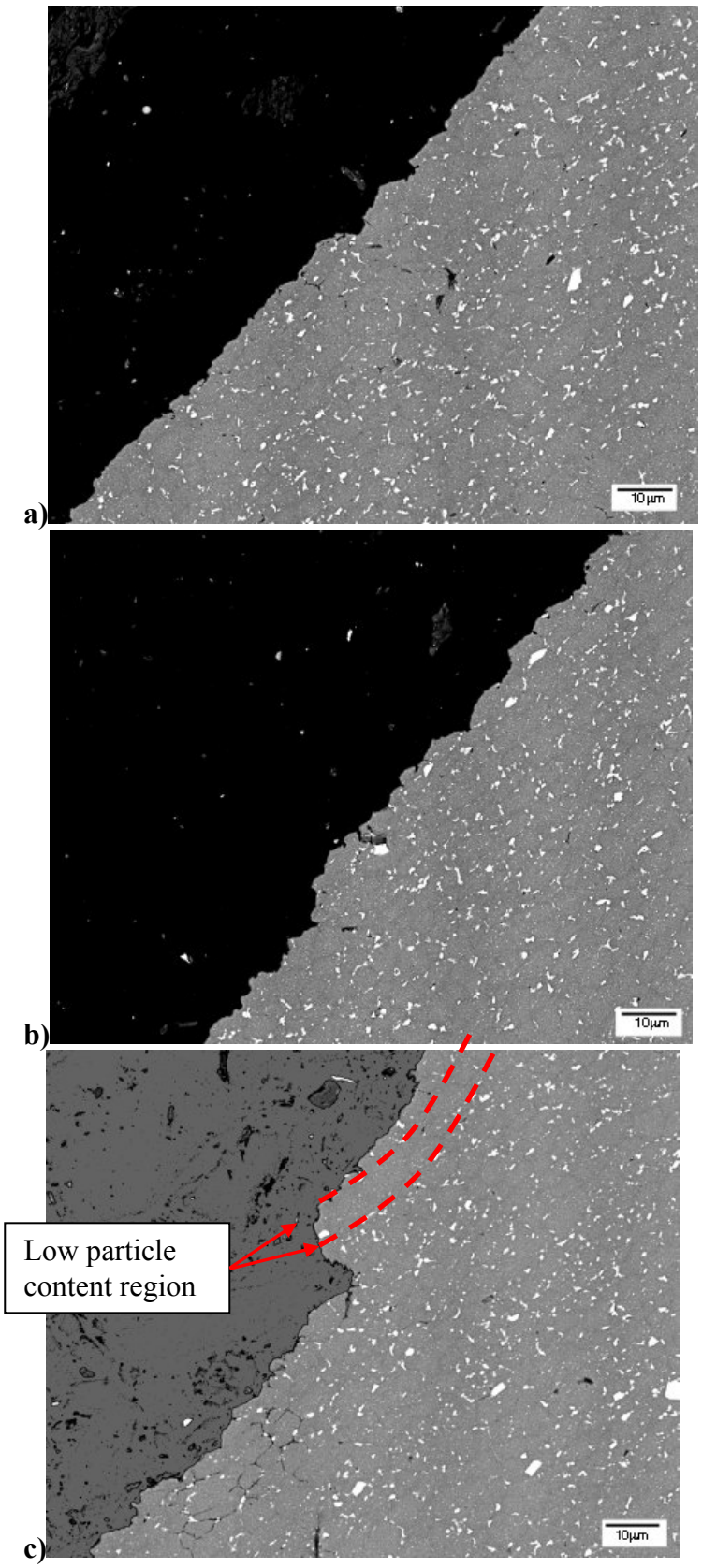

Fig. 11 Backscattered SEM image of the curved fracture path at the weld nugget: a) before step, b) after step and c) at step.

Fig. 11

REFERENCES

1 W.M. Thomas, E.D. Nicholas, J.C. Needham, M.G. Murch, P. Templesmith, and C.J. Dawes, 1991, "Friction Stir Butt Welding" Friction Stir Butt Welding. Int Patent App PCT/GB92/02203 and GB Patent App 9125978.8, December 1991. US Patent No. 5,460,317, October 1995

2 R.S. Mishra and Z.Y. Ma, Mater. Sci. Eng R, 2005, 50, 1-78

3 B.I. Bjørneklett, Ø. Frigaard, Ø. Grong, O.R. Myhr, and O.T. Midling, 1998, Proc. ICAA-6, Toyohashi, Japan, pp. 1531-1536

4 A.F. Norman, I. Brough, and P.B. Prangnell, 2000, Mater. Sci. Forum, Vols. 331-337, 1713-1718

5 K.V. Jata and S.L. Semiatin, Scripta Mater., 2000, 43, 743-749

6 R. W. Fonda, J. F. Bingert and K. J. Colligan, Scripta Mater. 51, 2004, 243-248

7 Ying Li, L. E. Murr and J. C. McClure, Mater. Sci. Eng. A, 1999, 271, 213-223

8 M.A. Sutton, B. Yang, A.P. Reynolds and R. Taylor, Mater. Sci. Eng. A, 2002, A323, 160-166

9 P. S. Pao, S. J. Gill, C. R. Feng and K. K. Sankaran, Scripta Mater., 2001, 45, 605-612

10 Yutaka S. Sato, Mitsunori Urata, and Hiroyuki Kokawa, Metall. Mater. Trans. 33A, 2002, 625

11 M.W. Mahoney, C.G. Rhodes, J.G. Flintoff, R.A. Spurling and W.H. Bingel, Metall. Mater. Trans., 1998, 29A, 1955-1964

12 H.G. Salem, Scripta Mater. 49, 2003, 1103-1110

13 B. Yang , J. Yan , M.A. Sutton and A.P. Reynolds, Mater. Sci. .Eng. A364, 2004, 55-65

14 M. A. Sutton, A.P. Reynolds, Junhui Yan, Bangcheng Yang and Ning Yuan, Eng. Fracture Mechanics, 2006, 73, 391-407

15 C. Genevois, A. Deschamps and P. Vacher , Mater. Sci. Eng. A, 2006, 415, 162-170

16 C. Genevois, A. Deschamps, A. Denquin and B. Doisneau-Cottignies, Acta Mater. **53,** 2005, 2447

17 M. Peel, A. Steuwer, M. Preuss and P. J. Withers, Acta Mater. 51, 2003, 4791-4801

18 D. Lohwasser, in: Proceedings of the Third International Friction Stir Welding Symposium, TWI, Kobe, Japan, 27–28 September 2001.

19 K. Colligan, K. McTernan and J.R. Pickens, in: Proceedings of the Third International Friction Stir Welding Symposium, TWI, Kobe, Japan, 27–28 September 2001

20 M.J. Starink, Int. Mater. Rev, 2004, Vol. 49, 191-226

21 K. Colligan, I. Ucok, K. McTernan, P.J. KonKol and J.R. Pickens, in: Proceedings of the Third International Friction Stir Welding Symposium, TWI, Kobe, Japan, 27–28 September 2001

22 D.P.P. Booth, PhD thesis, University of Southampton, Southampton, 2003

23 M.J. Starink, N. Gao, J.L. Yan, Mater. Sci. Eng. A, 2004, vol. 387-389, 222-22

24 M.J. Starink, N. Gao, L. Davin, J. Yan, A. Cerezo, Phil. Mag., 85, 2005, 1395-1418

25 N. Gao, L. Davin, S. Wang, A. Cerezo and M.J. Starink, Mater. Sci. Forum, 2002, vol. 396-402, pp 923-28

26 S.C. Wang, F. Lefebvre, J.L. Yan, I. Sinclair and M.J. Starink, Mater. Sci. Eng. A, 2006, Vol. 431, 123
27 M.J. Starink, A. Cerezo, N. Gao, J.L. Yan, Philosoph Mag Lett 86, 2006, 243-252
28 S.C. Wang, M.J. Starink and N. Gao, Scr. Mater., 2006, Vol. 54, 287-291
29 A.K. Jena, A.K. Gupta and M.C. Chaturvedi, 1989, Acta Metall., Vol. 37, No. 3, pp. 885-895
30 G.W. Smith, W.J. Baxter and R.K. Mishra, 2000, J. Mater. Sci., Vol. 35, pp. 3871-3880
31 J. Koike, M. Mabuchi and K. Higashi, Acta Metall., 1994, Vol. 43, 199-206
32 F. Lefebvre, S. Wang, M.J. Starink and I. Sinclair, Mater Sci Forum, 2002, vol. 396-402, pp 1555-1600
33 L.M. Wang, H.M. Flower and T.C. Lindley, Scripta Mater., 1999, 41, 391-396
34 V. Radmilovic, R. Killas, U. Dahmen, G.J. Shiflet, Acta Mater 1999; 47: 3987
35 S.C. Wang and M.J. Starink, Acta Mater, 2007, 55, pp 933-941.
36 K. Khor and I. Sinclair, 2002, Unpublished work, University of Southampton
37 Kh. A.A. Hassan, A.F. Norman and P.B. Prangnell, in: Proceedings of the Third International Friction Stir Welding Symposium, TWI, Kobe, Japan, 27–28 September 2001
38 M.J. Starink, S.C. Wang and I. Sinclair, 2005 TMS Annual Meeting held in San Francisco, California, February 13–17, 2005, in 'Friction Stir Welding and Processing III', Ed. Kumar V. Jata, M.W. Mahoney and R.S. Mishra (TMS, Warrendale, PA, USA, 2005) pp. 233-240
39 M.J. Starink and J.L. Yan, Materials Science Forum, 2006, Vol. 519-521, 251
40 A.F. Norman, I. Borough and P.B. Prangnell, 2000, Mater. Sci. Forum, Vol. 331-337, pp. 1713-1718
41 K.N. Krishnan, Mater. Sci. Eng. A, 2002, 327, pp. 246-251
42 K. Colligan, 1999, Proc. 1st International Symposium on friction stir welding, Thousand Oaks, California, 14-16 June
43 M.P. Thomas and J.E. King, Scr. Metall. Mater., 1994, vol 31, 209-214
44 M.P. Thomas, PhD Thesis, University of Cambridge, 1995
45 A.P. Reynolds, W.D. Lockwood and T.U. Seidel, 2000, Mater. Sci. Forum, Vol. 331-337, pp. 1713-1718
46 R. Rishi, Metall. Trans. A, 1981, 12A, pp. 1089-1097
47 Ø. Frigaard, Ø. Grong, S. Gulbrandsen-Dahl and O.T. Midling, 1999, Proc. 1st International Symposium on friction stir welding, Thousand Oaks, California, 14-16 June